DECONVOLUTION VERSUS CONVOLUTION – A COMPARISON FOR MATERIALS WITH CONCENTRATION GRADIENT

David Rafaja

Department of Electronic Structures, Faculty of Mathematics and Physics, Charles University, Ke Karlovu 5, CZ-121 16 Prague, E-mail: rafaja@karlov.mff.cuni.cz

Abstract

Efficiency of three deconvolution methods used in X-ray powder diffraction analysis is compared for materials with concentration gradient. The first deconvolution method shown in this comparison is a modification of the classical Stokes method. In two other methods, the re-convoluted intensities are fitted to the measured data using the least-square procedure. The deconvoluted profile is represented either by a linear combination of harmonic functions or by coefficients describing the decomposition of measured profile into the basis of instrumental functions.

The results of deconvolution methods are further compared with results of an alternative approach, which is a convolution of the instrumental profile with an analytical function describing the diffraction on samples with concentration gradient. In this case, tuneable parameters of the analytical function following from the microstructure model are varied to arrive at the best match between the measured and re-convoluted intensities.

Analysing diffraction profiles measured on materials with concentration gradient, the most reliable information on the concentration profile was obtained using a combination of the above approaches. The direct deconvolution was used to get basic information on the shape of concentration profiles. The final form of the concentration profiles was adjusted by refining free parameters of the diffusion model.

Keywords: X-ray powder diffraction, convolution, deconvolution, and concentration gradient.

1. Introduction

Decomposition of diffraction profiles is a typical task in the diffraction profile analysis. The main problem is to separate the instrumental broadening from the measured diffraction pattern in order to obtain the pure physical profile containing information on microstructure of the material. This means that the well-known equation for convolution

$$h(x) = f * g = \int_{-\infty}^{\infty} f(y)g(x-y)dy \qquad (1)$$

has to be solved for $f(y)$, which represents the shape of the physical profile. Function $h(x)$ describes the measured diffraction profile; $g(x\text{-}y)$ is the instrumental function (response of the apparatus). The instrumental function covers usually the line broadening due to the spectral width of radiation, angular resolution of the diffractometer optics as well as a variety of aberrations. Typical examples for aberrations causing the instrumental broadening in the conventional Bragg-Brentano geometry are the sample transparency and the local sample displacement due to the flat specimen.

There are two different approaches how to treat the experimental diffraction pattern affected by instrumental broadening. The first one employs direct deconvolution. The second one solves Eq. (1) through convolution of physical and instrumental profiles, assuming that the physical profile can be approximated by a function of a limited number of parameters, which follow from the microstructure model of the respective material. Although the latter approach based on convolutions becomes more and more frequently used in the last time (see, e.g., Refs. [1-4]), they are still numerous applications, for which the use of a deconvolution technique is inevitable. The reason is that a proper microstructure model cannot be built without an approximate knowledge of the deconvoluted profiles, an example of them being materials with concentration gradient.

Regarding the direct deconvolution of diffraction profiles, the excellent comprehensive overview of deconvolution methods by M. Čerňanský [5] can be recommended to the reader's attention. Among the large number of deconvolution methods discussed in [5], the most popular methods work with the least-square fitting of re-convoluted profiles to the measured intensities, see Ref. [6] and the references therein. The least-square method is suitable to solve integral equations of the first kind, which is also the case of the equation for convolution (1).

In this paper, three procedures used for deconvolution of powder diffraction patterns are compared. The Stokes method [7] working with smoothed experimental and instrumental data, decomposition of physical profiles into a Fourier series [6] and decomposition of experimental data into a linear combination of instrumental profiles. Materials with concentration gradients were selected for this comparison, as the presence of concentration profiles implies strongly asymmetrical physical broadening, which is not favourable for most deconvolution methods. Finally, a microstructure model was built for samples with concentration gradient, in which the corresponding physical profile was calculated. Free parameters of the microstructure model were refined to arrive at the best match between the experimental and the re-convoluted data.

2. Competing deconvolution procedures

2.1. Stokes method with Gaussian smoothing

The original Stokes method [7] utilises the well-known property of the Fourier transformation – the Fourier trans-

formation of convolution of two functions can be expressed as multiplication of Fourier transforms of these functions:

$$FT(h) = FT(f * g) = FT(f).FT(g) \qquad (2)$$

Thus, the pure physical function f can be obtained from the measured profile h and from the instrumental profile g using the formula:

$$f = FT^{-1}\left(\frac{FT(h)}{FT(g)}\right) = FT^{-1}\left(\frac{H}{G}\right) \qquad (3)$$

Throughout the text, the symbols FT and FT^{-1} denote the Fourier and the inverse Fourier transformation. The capitals F, G and H denote the Fourier transforms. Due to the ill-posed nature of deconvolution, which is caused mainly by the truncation of diffraction profile and by the presence of noise in both the experimental and instrumental data, the formula (3) does not yield useful results. The solution is oscillating as a rule; the amplitude of the oscillations being comparable with the maximum of the deconvoluted function.

In order to overcome problems with truncation of diffraction profiles, the experimental data must be pre-processed. In the first step, the background is subtracted and the missing marginal data are filled by zeros. To avoid problems with the noise, the input data are often smoothed. This means that typically the high-frequency noise is removed. Such a filtering of input data was used in the modified Stokes procedure presented in this contribution. Fourier transforms of both experimental and instrumental profiles were multiplied by Gaussian functions:

$$F' = \left[H \exp\left(-\frac{t^2}{\sigma_h^2}\right)\right] \Big/ \left[G \exp\left(-\frac{t^2}{\sigma_g^2}\right)\right] \qquad (4)$$

This corresponds to the following combination of the Fourier transforms:

$$F' = FT(f') = \frac{FT(h) \cdot FT(s_h)}{FT(g) \cdot FT(s_g)} = \frac{FT(h * s_h)}{FT(g * s_g)} \qquad (5)$$

The functions s_h and s_g are the inverse Fourier transforms of the Gaussian functions multiplying the functions H and G in Eq. (4). Further, it holds as a consequence of Eq. (5):

$$FT(h * s_h) = FT(f') \cdot FT(g * s_g) = FT(f' * g * s_g) \qquad (6)$$

Applying inverse Fourier transformation on Eq. (6), we will get a similar equation for convolutions:

$$f' * g * s_g = h * s_h = h * s_f * s_g \qquad (7)$$

The right hand of Eq. (7) was rewritten to arrive at formally same convolutions on the left and right side. The left and right hands of Eq. (7) are equal if

$$f' = f * s_f \qquad (8)$$

Equation (8) specifies the amount of smoothing in the deconvoluted profile. It can simply be shown that the deconvoluted profile is smoothed by the Gaussian function if both g and h are smoothed by Gaussian functions.

$$\begin{aligned} s_h = s_f * s_g &= FT^{-1}[FT(s_f) \cdot FT(s_g)] = \\ &= FT^{-1}\left[\exp\left(-\frac{t^2}{\sigma_f^2}\right) \cdot \exp\left(-\frac{t^2}{\sigma_g^2}\right)\right] = \\ &= FT^{-1}\left[\exp\left(-t^2 \cdot \frac{\sigma_f^2 + \sigma_g^2}{\sigma_f^2 \sigma_g^2}\right)\right] = FT^{-1}\left[\exp\left(-\frac{t^2}{\sigma_h^2}\right)\right] \end{aligned} \qquad (9)$$

Therefore, the smoothing parameter σ_f is given by reciprocal difference of the parameters σ_h and σ_g:

$$\sigma_f^2 = \frac{\sigma_g^2 \sigma_h^2}{\sigma_g^2 - \sigma_h^2} \qquad (10)$$

The smoothing parameter σ_f describes the filtering of the Fourier transform of the deconvoluted profile:

$$FT(f') = F' = F \exp\left(-\frac{t^2}{\sigma_f^2}\right) \qquad (11)$$

To derive the exact form of the smoothing function for f, we must perform the inverse Fourier transformation of Eq. (11):

$$f' = f * FT^{-1}\left[\exp\left(-\frac{t^2}{\sigma_f^2}\right)\right] = f * s_f, \qquad (12)$$

where

$$\begin{aligned} s_f &= FT^{-1}\left[\exp\left(-\frac{t^2}{\sigma_f^2}\right)\right] = \frac{1}{2\sqrt{\pi}} \int_{-\infty}^{\infty} \exp\left(-\frac{t^2}{\sigma_f^2}\right) = \\ &= \frac{1}{2\sqrt{\pi}} \sigma_f \exp\left(-\frac{x^2 \sigma_f^2}{4}\right) \end{aligned} \qquad (13)$$

It follows from Eq. (13) that the smoothing function is Gaussian in form. The area below the function s_f is equal to unity,

$$\int_{-\infty}^{\infty} s_f \, dx = \frac{\sigma_f}{2\sqrt{\pi}} \int_{-\infty}^{\infty} \exp\left(-\frac{x^2 \sigma_f^2}{4}\right) dx = 1, \qquad (14)$$

if the inverse Fourier transformation is defined by the formula:

$$FT^{-1}(F) = \frac{1}{2\pi} \int_{-\infty}^{\infty} F(t) \exp(itx) \, dt \qquad (15)$$

In such a case, the smoothing has no effect on the total integrated intensity of the deconvoluted profile.

Equation (10) has several important consequences. The deconvoluted profile is automatically smoothed if the experimental data and the instrumental profile are smoothed. For correct smoothing, σ_h must be less than σ_g, which means that the experimental function *h* must be filtered to lower frequencies than the instrumental function *g*. If σ_h and σ_g have approximately the same value, σ_f is very high; thus, the physical function *f* is not smoothed at all. If σ_g is much larger than σ_h, the smoothing of *f* is extreme – it is the same as the smoothing of *h*.

The computer code for deconvolution routine based on the modified Stokes method was written in the MATLAB® environment. Fourier transforms were calculated using the internal MATLAB® function for the fast Fourier transformation and the inverse Fourier transformation.

2.2. Decomposition of experimental profiles using Fourier expansion

The second procedure tested in this paper is the decomposition of diffraction profiles using expansion of the physical functions into the Fourier series. This approach is especially advantageous if the subsequent method of data reduction works with the Fourier coefficients, for instance if the Warren-Averbach analysis is applied. The computing routine used in the test is completely based on the technique, published by Sánches-Bajo and Cumbrera [6]. The only exception is that we took the instrumental profile in its measured form, instead of approximating it by an expansion into the Hermite polynomials like in [6]. Employing the expansion of the pure physical profile into a Fourier series, function *f* takes the form:

$$f(x)=\sum_{j=0}^{m} C_j \cos(j\omega_0 x)+\sum_{j=1}^{m} S_j \cos(j\omega_0 x) \text{ with } \omega_0 =\frac{2\pi}{\Delta} \tag{16}$$

The symbol Δ in Eq. (16) defines the interval, in which the experimental profile was measured. Regarding the equation for convolution (1), the experimental profile can be written as

$$\begin{aligned} h(x) &= \int_{-\infty}^{\infty} g(x-y)\cdot\left[\sum_{j=0}^{m} C_j \cos(j\omega_0 y)+\sum_{j=1}^{m} S_j \sin(j\omega_0 y)\right]dy = \\ &= \sum_{j=0}^{m} C_j \int_{-\infty}^{\infty} g(x-y)\cos(j\omega_0 y)\,dy + \\ &+ \sum_{j=1}^{m} S_j \int_{-\infty}^{\infty} g(x-y)\sin(j\omega_0 y)\,dy \end{aligned} \tag{17}$$

Equation (17) represents convolutions of the instrumental function *g* with the basis of harmonic functions:

$$h(x)=\sum_{j=0}^{m} C_j [g*\cos(j\omega_0 y)]+\sum_{j=1}^{m} S_j [g*\sin(j\omega_0 y)] \tag{18}$$

Within the deconvolution procedure, Eq. (18) is solved for coefficients C_j and S_j in the least-square sense. Application of this deconvolution routine implies also an automatic smoothing of deconvoluted data. The amount of smoothing is determined by a number of harmonic functions (*m* in Eq. (16)-(18)). The lower *m*, the higher is the degree of smoothing.

The related computer code was written in the MATLAB® environment. The convolutions in Eq. (18) were calculated with the aid of the fast Fourier transformation and the inverse fast Fourier transformation (see Eq. (2)). The least-square refinement of the coefficients C_j and S_j is performed successively for increasing number of harmonic functions, *m*. Because of the large expected asymmetry of the deconvoluted profiles in samples with concentration gradient, the harmonic functions up to the 40th order were tested. The best set of C_j and S_j was selected according to the lowest sum of residuals between the original data *h* and the re-convoluted data *h*' obtained from the back convolution:

$$S=\sum_{n=1}^{N}[h'(x)-h(x)]^2=\sum_{n=1}^{N}[f*g-h]^2=\min \tag{19}$$

The deconvoluted profile is calculated from Eq. (16). The summation in Eq. (19) is performed over all experimental data.

2.3. Experimental profile regarded as a linear combination of instrumental profiles

The last deconvolution procedure compared here solves the equation for convolution (1), rewritten into the form used for discrete data:

$$h_m=\sum_{-\infty}^{\infty} f_n g_{m-n} \tag{20}$$

In the matrix representation, Eq. (20) takes the form:

$$\begin{pmatrix} g_0 & g_{-1} & g_{-2} & g_{-3} & \cdots \\ g_1 & g_0 & g_{-1} & g_{-2} & \cdots \\ g_2 & g_1 & g_0 & g_{-1} & \cdots \\ g_3 & g_2 & g_1 & g_0 & \cdots \\ \vdots & \vdots & \vdots & \vdots & \ddots \end{pmatrix} \begin{pmatrix} f_1 \\ f_2 \\ f_3 \\ f_4 \\ \vdots \end{pmatrix} = \begin{pmatrix} h_1 \\ h_2 \\ h_3 \\ h_4 \\ \vdots \end{pmatrix} \tag{21}$$

Consequently, the Dirac δ-function corresponds to an identity matrix for the instrumental profile and to a single "one" embedded in a zero matrix for the physical profile. However, Eq. (20) represents an infinite system of linear equations. Moreover, the system of equations is underestimated, as the data contain noise (random errors). Therefore, an assumption must be done to reduce the number of equations (the number of parameters) in the linear combination (20).

In contrast to the deconvolution procedures employing the Fourier analysis, we can assume here that the deconvoluted intensities are equal to zero outside a certain range. This assumption reduces substantially the number of columns in the **G** matrix in Eq. (21). It means that the system of linear equations (20) becomes overestimated. Thus,

it can be solved using the least-square method. However, it is still necessary to filter the noise in the deconvoluted data. For filtering, the Fourier smoothing or the Golay-Savitzky method [8] were alternatively applied. The Fourier smoothing means a convolution of the deconvoluted profile with a Gaussian function like in the modified Stokes method described above. The Golay-Savitzky method represents the direct smoothing in the reciprocal space.

2.4. Refinement of free parameters of the diffusion model

A simple diffusion model was used to describe the concentration profiles in the samples. One-dimensional diffusion with concentration-independent diffusion coefficients in crystallites having the same size was assumed. In that case, the concentration profile takes the form of the error function (see, e.g. [9]),

$$c = \mathrm{erfc}(x / \sqrt{Dt}), \tag{22}$$

where x means the distance in individual crystallites (in individual diffusion couples), D the diffusion coefficient and t the diffusion time. The dominant factor modifying the shape of concentration profiles and therefore the shape of the corresponding diffraction profiles is the ratio of the total length of diffusion couples to the square root of Dt. For the concentration ranges investigated here, all particular components (TiN, TiC, Ti (C, N), (Ti, Mo) C, (Ti, Mo)(C, N) and MoC_{1-x}) crystallise with the face-centred cubic structure. Their lattice parameters follow the Vegard rule quite well [10]. Thus, the dependence of the interplanar spacing on the concentration is represented by the linear function:

$$d = d_0 + d_1 c \tag{23}$$

In Eq. (23), d_0 represents the interplanar spacing for $c = 0$, d_1 the change in interplanar spacing with the concentration of in-diffusing or out-diffusing species. Neglecting the macroscopic concentration depth profile in the sample, the influence of absorption of radiation on the shape of diffraction profiles can be omitted. Then the diffracted intensities depend linearly on the differential volume of material having a certain concentration:

$$I(\sin\theta) \propto V = \frac{dx}{d(\sin\theta)} = \frac{dx}{d(\lambda / 2d)} \tag{24}$$

The last part of Eq. (24) follows from the Bragg equation. In a further step, additional line broadening due to the small size of crystallites must be taken into account. Thus, the diffraction profiles calculated according to Eq. (24) were convoluted with the Cauchy function:

$$y = \frac{w}{\pi(x^2 + w^2)} \tag{25}$$

Its area is normalised to unity. The Cauchy function should be exchanged by the Gaussian function if the additional physical broadening is caused by micro-stress rather than by the small size of crystallites. In Eq. (25), diffraction angle, x, is calculated in the units sin θ; the same units are used also for the width of the Cauchy function, w. The above model is characterised by five free parameters ($K = \sqrt{(Dt)}$, d_0, d_1, w and a scale factor normalising the calculated intensities to the experimental ones). Note, that a physically true model should include two parameters more: the minimum and the maximum concentration of the in-diffusing species. However, the minimum and the maximum concentrations would strongly correlate with the parameter of the diffusion model, K, and with the parameters d_0 and d_1. Therefore, the parameters related to the interplanar spacing should not be refined in a true model. They should be taken from an independent experiment. On the contrary, it can be shown that variation in the minimum and maximum concentrations has a similar influence on the shape of the resulting diffraction profile like the changes in d_0 and d_1.

Upon refinement, the linear least-squares method was iteratively applied to the first-order Taylor expansion of the calculated diffraction profile:

$$S = \sum_n \left[I^{meas} - \left(I_0^{calc} + \sum_j \frac{\partial I^{calc}}{\partial p_j} \Delta p_j \right) \right]^2 = \min \tag{26}$$

The increments to the refined parameters, Δp_j, follows from the solution of the matrix equation:

$$\left\| \sum_n \frac{\partial I^{calc}}{\partial p_i} \frac{\partial I^{calc}}{\partial p_j} \right\| \cdot \| \Delta p_i \| = \left\| \sum_n (I^{meas} - I_0^{calc}) \frac{\partial I^{calc}}{\partial p_i} \right\| \tag{27}$$

All convolutions were calculated numerically using the fast Fourier transformation and the inverse fast Fourier transformation (according to Eq. (2)).

3. Experimental details

X-ray diffraction experiments were performed with a conventional Bragg-Brentano diffractometer (XRD-7, Seifert/Freiberger Präzisionsmechanik). The nickel-filtered radiation of copper anode with a divergence of 1° was transmitted by a Soller collimator in primary beam and diffracted on the sample. The optics of the diffracted beam consisted of a secondary Soller collimator and the receiving slit of 0.15 mm. The selected angular range was scanned repeatedly with the step size of 0.01° in 2θ. The total counting time exceeded 60 seconds per step. To arrive at a good experimental resolution, reflections in the high-angle region were selected for the measurement.

The instrumental broadening was measured on the standard sample of cubic LaB_6 offered by NIST. The instrumental profile measured on the diffraction line (332) is shown in Fig. 1. The measurement was carried out in the same diffraction geometry and with the same instrumental parameters, which were used for samples with concentration gradient. For the standard, the counting time was 20

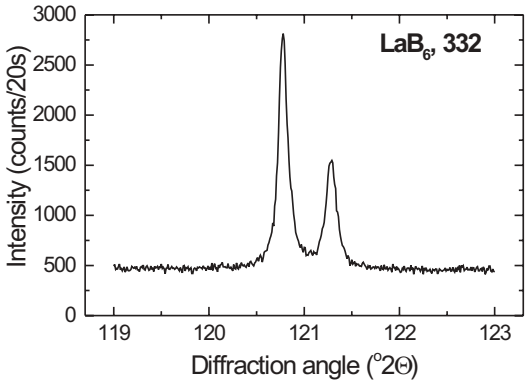

Figure 1. Instrumental broadening measured on the reflection (332) of cubic LaB_6.

seconds per step. To avoid problems with different angular separation of spectral lines in the $K\alpha_1/K\alpha_2$ doublet due to different diffraction angles of the respective materials, the data were first converted into the equidistant scale in sin θ.

The following samples were used to test the deconvolution procedures – cubic TiC_{1-x}, hexagonal Mo_2C, ternary mixture (Ti_x Mo_{1-x}) C and quaternary mixture (Ti_x Mo_{1-x}) (C_y N_{1-y}). According to the chemical analysis, TiC_{1-x} contained 19.33 weight percent of carbon, this corresponds to the stoichiometric ratio $TiC_{0.96}$. The analysed composition of the MoC_{1-x} powder was $MoC_{0.51}$ (5.72 weight percent of carbon). The ternary ($Ti_{0.85}$ $Mo_{0.15}$) C was produced by hot pressing $TiC_{0.96}$, $MoC_{0.51}$ and graphite in argon atmosphere at 2000°C. Afterward, it was annealed in argon for 16 days at 1450°C. The last three samples with the nominal composition ($Ti_{0.75}$ $Mo_{0.25}$) ($C_{0.75}$ $N_{0.25}$) were prepared by hot pressing the mixture of 50 mole of ($Ti_{0.5}$ $Mo_{0.5}$) C and 50 mole of Ti ($C_{0.5}$ $N_{0.5}$) in argon atmosphere at 2000°C. Subsequently, two of these three samples were annealed for 48 and 192 h, respectively, at 1450°C in one bar Ar.

4. Results and discussion

4.1. Comparison of deconvolution procedures

All deconvolution procedures outlined above yielded very similar results for the majority of experimental data. Nevertheless, if we compare only the differences between the experimental and the re-convoluted data, the most successful deconvolution routine was that based on the linear combination of instrumental profiles (Section 2.3.). Furthermore, the main difference between individual procedures follows from the amount of smoothing, which is automatically included in the respective deconvolution routine. The quality of deconvoluted patterns (and the match between the re-convoluted and the experimental intensities) depends on the shape of physical profile. If the physical broadening is much larger than the instrumental one, also the deconvolution procedures with high amount of smoothing (e.g., the decomposition using Fourier expansion with a small number of Fourier coefficients) yield excellent results. This can be illustrated on the hot-pressed non-annealed quaternary ($Ti_{0.75}$ $Mo_{0.25}$) ($C_{0.7}$ $N_{0.3}$). After deconvolution, three distinct intensity maxima are clearly visible at 122.49°, 123.09° and 123.75° (Fig. 2). These peaks indicate the presence of two (Ti, Mo) (C, N) phases, which are usually denoted as Ti-rich α'–(Ti, Mo) (C, N) (here with the lattice parameter a = 4.2921 Å) and Mo-rich α"–(Ti, Mo) (C, N) (here with a = 4.3044 Å), and the presence of non-stoichiometric cubic $MoC_{0.74}$ (a = 4.2788 Å) [11].

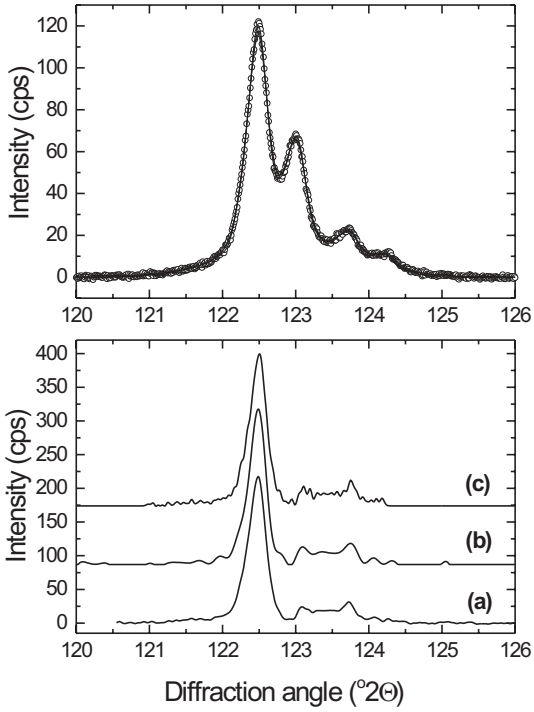

Figure 2. Experimental data (open circles) and re-convoluted intensities (solid line) measured with the hot-pressed quaternary ($Ti_{0.75}$ $Mo_{0.25}$) ($C_{0.7}$ $N_{0.3}$) (Figure at the top). At the bottom: physical profiles obtained from the experimental data by using the Stokes method (a), the Fourier expansion (b) and the linear combination of instrumental profiles (c).

On the other hand, the Stokes deconvolution with Gaussian smoothing (Section 2.1.) was the most successful routine in extreme cases, when the shape of the experimental profile approached the shape of the instrumental profile. Generally, this method yields the best results if the pure physical profile is very narrow. Such a diffraction profile was measured with the TiC powder (Fig. 3). Only two deconvolution procedures (the Stokes method and the linear combination of instrumental profiles) are compared here. The reason is that the decomposition of the diffraction profile into a series of harmonic functions did not yield a convergent solution up to the 40th order of Fourier coefficients. Linear combination of instrumental profiles yielded apparently much smoother deconvoluted profile than the Stokes method. However, the level of smoothing for the linear combination was too high, which affected the shape

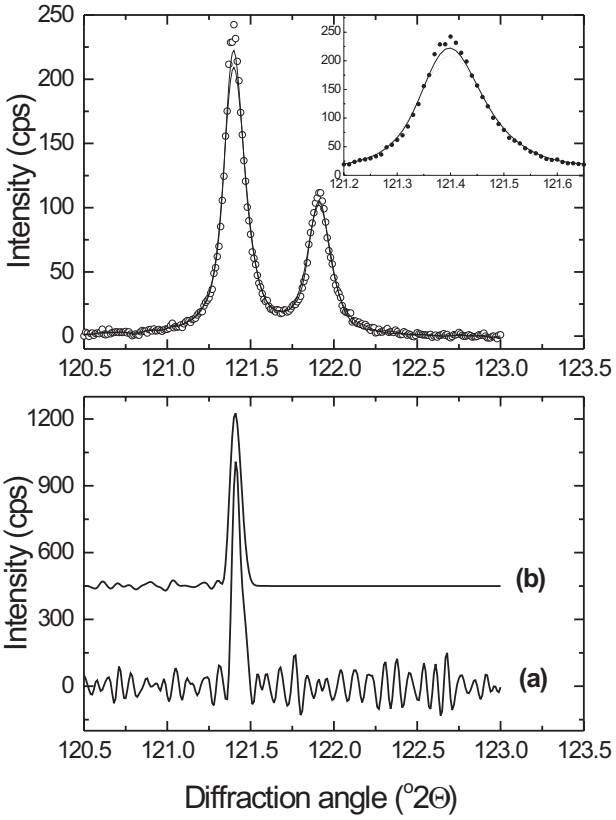

Figure 3. Figure at the top: experimental data (open circles) and re-convoluted intensities (solid lines) measured with $TiC_{0.96}$. Figure at the bottom: deconvoluted profiles obtained using the Stokes method (a) and the linear combination of instrumental profiles (b). The differences between the re-convoluted profiles and the experimental data are shown in the inset (solid line is for the Stokes method, dashed line for the linear combination of instrumental efffects).

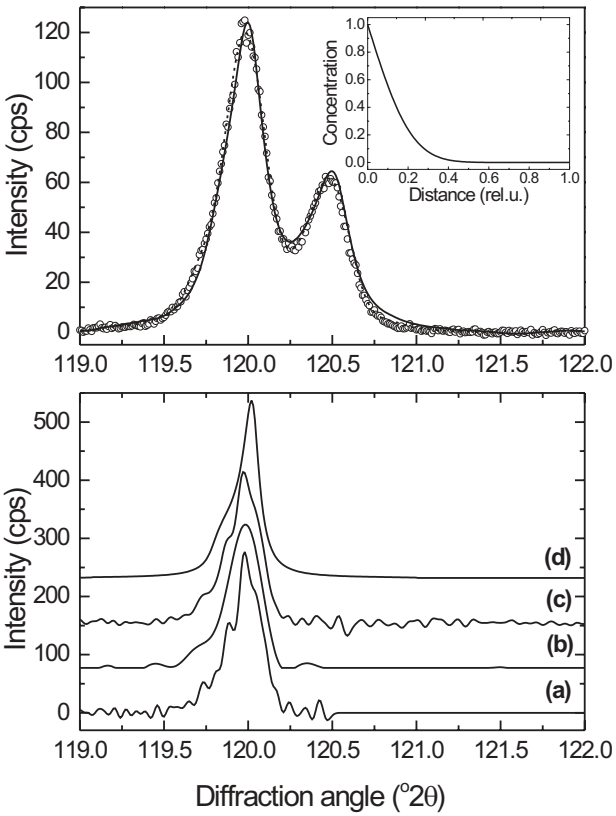

Figure 4. At the top: diffraction profile measured on the (105) reflection of hexagonal $MoC_{0.51}$ (open circles) compared with the re-convoluted profile (dashed line) and with the diffraction profile obtained from the concentration profile fitting (solid line). Inset: the calculated shape of the concentration profile of carbon. On the concentration scale, "0" means the minimum carbon concentration, "1" the maximum one. At the bottom: physical profiles obtained from deconvolution by using linear combination of instrumental profiles (a), Fourier expansion (b), Stokes method (c) and concentration profile fitting (d).

of the re-convoluted profile. The re-convoluted peak was broader than from the Stokes method having a lower maximum (see inset to Fig. 3).

From the point of view of the computer time consumption, the Stokes method is the fastest one, followed by the Fourier decomposition. The slowest method is the decomposition of experimental profiles into the linear combination of instrumental profiles, as large matrix equations are solved upon this approach. In particular cases, the most efficient technique is the concentration profile fitting (Section 2.4.), which works with convolutions of the physical profile calculated using equations (22) – (24) with the Cauchy function (25) and with the instrumental profile. Results of this method are reported in the next Section.

4.2. Results of the concentration profile fitting

The concentration profile fitting can be regarded as a method, which yields physically reliable information on the real composition and the real structure of the sample. However, its use is limited to the cases, in which an appropriate diffusion model can be created. Employing this technique, it is useful if the concentration profile fitting succeeds a deconvolution method in order to get fundamental characteristics of the diffusion model. In this test, this approach was first applied to study the homogeneity of the hexagonal $MoC_{0.51}$ powder. The shape of the deconvoluted profile (Fig. 4) is characteristic for a presence of a steep concentration gradient in the sample. Bulk of the sample has the lattice parameters a = (3.01028 ± 0.00004) Å and c = (4.73569 ± 0.00004) Å, which yield the interplanar spacing of 0.8902 Å for the (105) planes. The above lattice parameters are the result of Rietveld refinement. The profile asymmetry towards smaller diffraction angles (towards larger interplanar spacing and lattice parameter) agrees well with the positive slope, which describes the dependence of lattice parameters in MoC_{1-x} on the carbon concentration [11]. The concentration profile fitting yielded the minimum and the maximum interplanar spacing (for the minimum and the maximum carbon concentration) d_{min} = 0.8893 Å and d_{max} = 0.8903 Å.

Another sample with a concentration gradient had the average composition of $(Ti_{0.85}\,Mo_{0.15})\,C$. From the shape of the diffraction profile, it is evident that the concentration profile is much broader than in the previous case (with respect to the size of the diffusion couple), which indicates an approaching diffusion process (Fig. 5). The lattice parameter for the lowest concentration of molybdenum in the sample is equal to 4.3192 Å, which is lower than the lattice

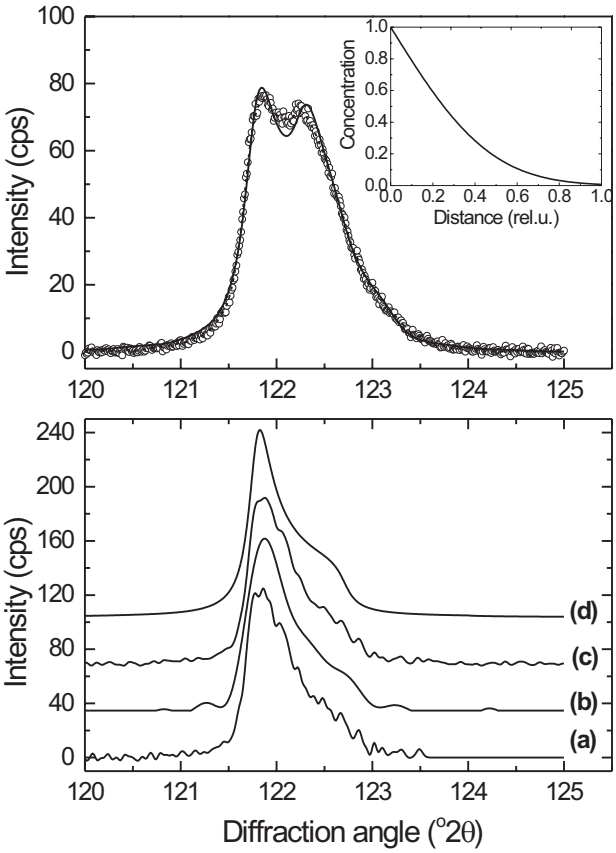

Figure 5. At the top: the intensity band measured on the (422) line of ($Ti_{0.85}$ $Mo_{0.15}$) C (open circles). The re-convoluted profile is indicated by the dashed line; the diffraction profile obtained from the concentration profile fitting is indicated by the solid line. The schematic shape of the concentration profile is shown in the inset. At the bottom: physical profiles obtained from linear combination of instrumental profiles (a), from the Fourier expansion (b), from the Stokes method (c) and from the concentration profile fitting (d).

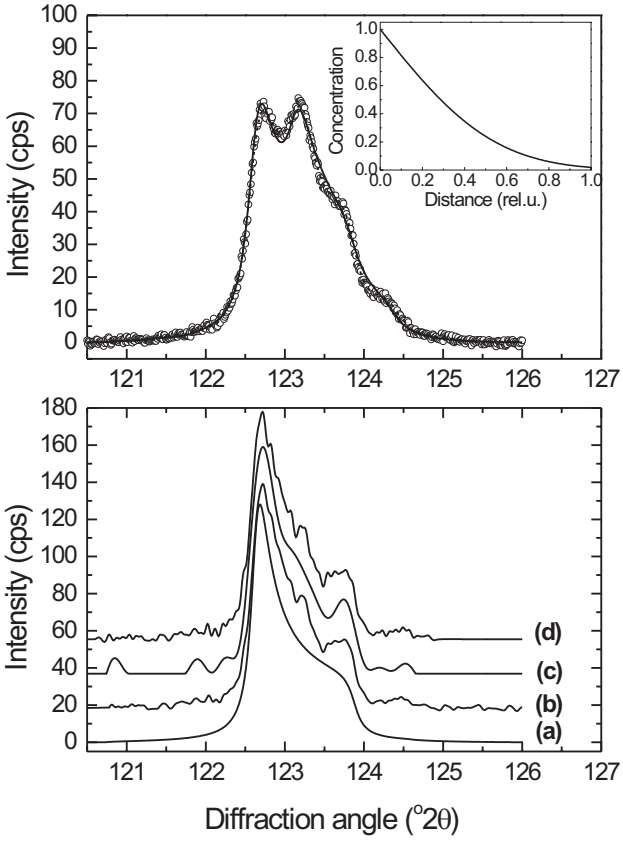

Figure 6. Diffraction profile measured with quaternary ($Ti_{0.75}$ $Mo_{0.25}$) ($C_{0.7}$ $N_{0.3}$) annealed for 48 h at 1450°C in argon atmosphere (open circles). The re-convoluted diffraction profile is plotted by dashed line, the diffraction profile corresponding to the concentration profile shown in the inset by the solid line. At the bottom: physical profiles obtained from the concentration profile fitting (a), from the Stokes method (b), from the Fourier expansion (c) and from the linear combination of instrumental profiles (d).

parameter of TiC (a = 4.3278 Å). This confirms that increasing amount of molybdenum in the host structure of TiC decreases the lattice parameter of the ternary face centred cubic (Ti_x, Mo_{1-x}) C phase. The lattice parameter corresponding to the highest analysed concentration of molybdenum in the sample is 4.2996 Å. As the concentration profile is related to the concentration of molybdenum, the change of lattice parameter (change of the interplanar spacing) with concentration is negative, which implies the physical line broadening toward higher diffraction angles.

The last two examples illustrate the influence of increasing diffusion time on the shape of diffraction and concentration profiles. The "overall" composition of both samples was ($Ti_{0.75}$ $Mo_{0.25}$) ($C_{0.7}$ $N_{0.3}$), the same as for the first sample presented in Section 4.1. The samples were annealed for 48 or 192 h at 1450°C in one bar Ar. In the first one, the deconvolution procedures discovered presence of two (Ti, Mo) (C, N) phases and a MoC_{1-x} phase (Fig. 6). The phase composition is similar to that in the non-annealed sample. After annealing the sample for 48 h at 1450°C, the titanium-rich α'–(Ti, Mo) (C, N) had the lattice parameter a = 4.2897 Å, the molybdenum-rich α"–(Ti, Mo) (C, N) the lattice parameter a = 4.2997 Å. The non-stoichiometric cubic MoC_{1-x} had the lattice parameter a = 4.2790 Å, which corresponds to the stoichiometric ratio x = 0.74 within experimental accuracy. The concentration profile fitting yielded a similar shape of the physical profile like the deconvolution routines. However, as a simple diffusion model assuming only presence of a single phase with a concentration gradient was employed, the re-convoluted diffraction profile did not fit the experimental data properly. The discrepancy can be also seen on the too wide range of lattice parameters obtained from the concentration profile fitting. The lattice parameter for the minimum concentration of titanium is 4.3018 Å, that for the maximum concentration of Ti 4.2761 Å.

The deconvoluted pattern of the latter sample annealed for 192 h (Fig. 7) indicates presence of the residual MoC_{1-x} with the lattice parameter 4.2770 Å. This value corresponds to a slightly lower carbon content in MoC_{1-x}, x = 0.73. The deconvoluted diffraction profiles of the quaternary (Ti, Mo) (C, N) build a continuous band starting at the diffraction angle of 122.80° and ending at 123.26°. The corresponding limits for the lattice parameters are 4.2980 Å for the molybdenum-rich α"–(Ti, Mo) (C, N) and 4.2887

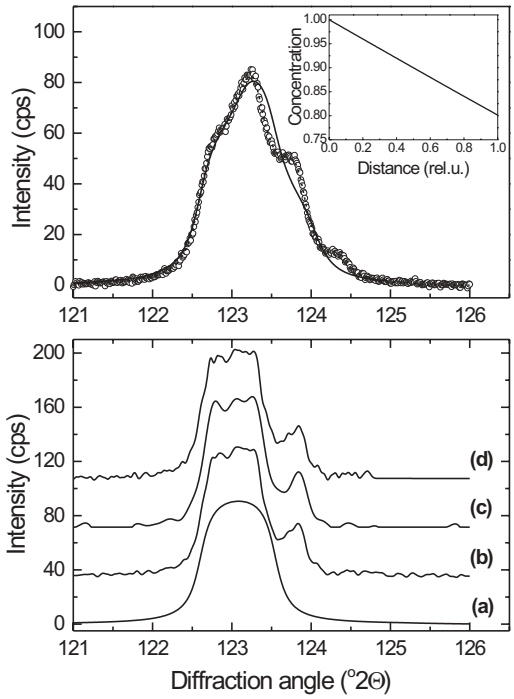

Figure 7. Diffraction profile measured with the quaternary ($Ti_{0.75}Mo_{0.25}$) ($C_{0.7}N_{0.3}$) annealed for 192 h at 1450°C in argon atmosphere (open circles). The re-convoluted diffraction profile (plotted by dashed line) reconstructs the experimental data quite well. The difference between the diffraction profile calculated for the concentration profile shown in the inset (plotted by solid line) and the experimental data is much larger, which is due to the simplicity of the structure model. Figure at the bottom shows physical profiles obtained from the concentration profile fitting (a), from the Stokes method (b), from the Fourier expansion (c) and from the linear combination of instrumental profiles (d).

Å for the titanium-rich α'–(Ti, Mo) (C, N). Typically, the physical profile takes a form of a continuous band if infinitesimal diffracting volumes are the same for all concentrations. This happens if the concentration profile is flat; i.e. if it can be approximated by a linear function. This is the case for "saturated" diffusion at longer diffusion times. As in the previous case, ignoring the presence of the residual MoC_{1-x} in the diffusion model increases the range of lattice parameters obtained from the concentration profile fitting. The analysed minimum and maximum concentrations were a_{min} = 4.2829 Å and a_{max} = 4.3020 Å.

5. Concluding remarks

Comparison of three deconvolution procedures has shown that the deconvoluted physical profiles differ only in extreme cases, when a high degree of smoothing is unfavourable. This is the case, for instance, if the pure physical profile is very narrow (approaching the Dirac δ-distribution), or if one of the edges of the physical profile is very steep. Steep edges of physical profiles are particularly characteristic for materials with concentration profile, which has a negligible line broadening due to the crystallite size or microstrain.

Comparison of the deconvolution procedures with concentration profile fitting illustrated the powerfulness of the concentration profile fitting. However, the reliability of results strongly depends on suitability of the microstructure model. Thus, a combination of both techniques shall be recommended. A deconvolution method should be applied to get preliminary data, which are necessary to build an appropriate microstructure model. For the final refinement of the model, the fitting of calculated diffraction profiles on the experimental data yields more reliable results than the deconvolution.

Acknowledgements

The author would like to thank to Dr. Pablo Wally (Vienna University of Technology, Austria) for supplying the samples. The financial support of the project # GAUK-154/99 by the Grant Agency of the Charles University Prague is greatly appreciated.

References

1. P. Scardi: A new whole powder pattern fitting approach *in* R.L. Snyder, J. Fiala and H.J. Bunge (ed.), *Defect and Microstructure Analysis by Diffraction*, International Union of Crystallography, Oxford University Press, 1999.
2. P. Scardi and M. Leoni, *J. Appl. Cryst.* **32** (1999) 671.
3. Y.H. Dong and P. Scardi, *J. Appl. Cryst.* **33** (2000) 184.
4. J.I. Langford, D. Louër and P. Scardi, *J. Appl. Cryst.* **33** (2000) 964.
5. M. Čerňanský: Restoration and preprocessing of physical profiles from measured data *in* R.L. Snyder, J. Fiala and H.J. Bunge (ed.), *Defect and Microstructure Analysis by Diffraction*, International Union of Crystallography, Oxford University Press, 1999.
6. F. Sánchez-Bajo and F.L. Cumbrera, *J. Appl. Cryst.* **33** (2000) 259.
7. A.R. Stokes, *Proc. Phys. Soc.* **61** (1948) 382.
8. A. Savitzky and M.J.E. Golay, *Anal. Chem.* **36** (1964) 1627.
9. J. Crank: *The Mathematics of Diffusion*, 2nd ed., Oxford University Press, Oxford, United Kingdom, 1987.
10. P. Wally, PhD Thesis, Vienna University of Technology, 1995.
11. E. Rudy, *Journal of the Less-Common Metals* **33** (1973) 43.